ANALYSIS OF THE GOLF/SOHO SOLAR OSCILLATION SPECTRUM

Alexandre Barbosa*

*Departamento de Física, Instituto Superior Técnico (Universidade de Lisboa)

alexandre.barbosa@tecnico.ulisboa.pt

November 23, 2022

ABSTRACT

A spectrum of solar oscillations corresponding to six months of continuous measurements of the GOLF instrument aboard SoHO is obtained and analysed. We identify the frequencies of the most penetrating $l \leq 3$ acoustic p-modes, the large and small separations and compare them with theoretical predictions coming from solar models. We find $\langle \Delta\nu_\odot \rangle = (135.41 \pm 0.66)$ μHz and $\langle \delta\nu_\odot \rangle = (8.67 \pm 0.35)$ μHz, consistent within 1.3σ with results from the VIRGO experiment. We examine the linewidths as a function of frequency and represent the observed modes in Echelle format. Finally, we pinpoint the Sun in an asteroseismic Hertzprung-Russel diagram, and discuss how stellar parameters can be inferred from these separations in solar-like oscillators.

1 INTRODUCTION

Analysing stellar oscillations allows astrophysicists to probe the interior of stars, uncovering their structure and dynamics by estimating stellar parameters with unparalleled precision.

The ongoing GOLF (Global Oscillations at Low Frequencies) experiment on the ESA/NASA SoHO (Solar and Heliospheric Observatory) mission, located in the vincinity of the Sun-Earth system lagrange point L1, was designed to study the internal structure of the Sun by measuring global solar oscillations.

In essence, GOLF measures the Doppler shift of the solar Na D spectral lines, and compares them to a standard given by the sodium vapour cell within the GOLF instrument [1].

After transversing this cell, a narrow region of the solar ressonance line is caught in a light trap, and the light scattered by the vapour within the cell perpendicularly is collected by two symetrically opposed photomultipliers. A longitudinal magnetic field is applied to the cell, so the absorption line is Zeeman split, and this displacement is related to the amplitude of a point in the blue and red wings of the solar profile [2].

Currently, GOLF is locked into blue wing operation mode due to equipment malfunction, to mantain a full duty cycle [3].

The modes of solar oscillation can be classified as p-modes, where the restoring force is pressure, with frequencies from 1 to 5 mHz, and g-modes, corresponding to internal gravity waves, where the restoring force is buoyancy and whose reported detection [4] [5] has been challenged [6] [7].

A perturbation of a spherical, non-rotating star that leads to radial oscillations can be described by a superposition of eigenmodes with frequencies ν_{nlm}, where $l < n$ and $-l < m < l$.

In spherical coordinates, we can write hence the pressure as

$$p(r,\theta,\phi,t) = \sum_{n,l,m} A_{nlm} r^{-1} \Psi_n(r) Y_l^m(\theta,\phi) e^{2\pi i \nu_{nlm} t} \quad (1)$$

where A_{nlm} is the mode amplitude, Ψ_n is the radial eigenfunction, Y_l^m is a spherical harmonic and we assume a $2l$+1-fold degeneracy for every value of the azimuthal order m.

At low degrees ($n >> l$), the p-mode frequencies satisfy [8]

$$\nu_{nl} \approx (n + l/2 + \alpha)\Delta\nu - A\frac{l(l+1)+\delta}{n+l/2+\alpha} \quad (2)$$

where α depends on the reflecting properites of the surface whereas δ on internal properties of the Sun, and

$$\Delta\nu = \Big(2\int_0^{R_\odot} \frac{dr}{c}\Big)^{-1} \quad (3)$$

is the large separation, inverse of the sound travel time through the diameter of the Sun, corresponding to the uniform spacing

$$\Delta\nu \approx \nu_{n,l} - \nu_{n-1,l} \quad (4)$$

In the second term, with $c \propto \sqrt{T/\mu}$ as the sound speed, where T is the temperature and μ the average molecular weight,

$$A = \frac{1}{4\pi^2}\Big(\frac{c(R_\odot)}{R_\odot} - \int_0^{R_\odot} \frac{dr}{r}\frac{dc}{dr}\Big) \quad (5)$$

leads, for low degrees, to the small frequency separation [9]

$$\delta\nu = \nu_{n+1,l} - \nu_{n,l+2} \approx -(4l+6)\frac{\Delta\nu}{4\pi^2\nu_{nlm}}\int_0^{R_\odot}\frac{dr}{r}\frac{dc}{dr} \quad (6)$$

2 GOLF/SoHO Data Analysis

2.1 Velocity Dispersion

The GOLF experiment records variations in the Sun's luminosity, whence it infers the surface velocity dispersion, which is Fourier transformed to obtain the solar oscillation spectrum.

We plot the velocity dispersion using data corresponding to the first 183 days of GOLF operation, from April 11th 1996 to October 10th 1996 for two photo-multipliers, labelled PM1 and PM2, in figure 1. In total, this time series contains 790560 data points, with a sampling time of 20 seconds; the first point is centered at 00h00m9.5s April 11th 1996 (UT Time).

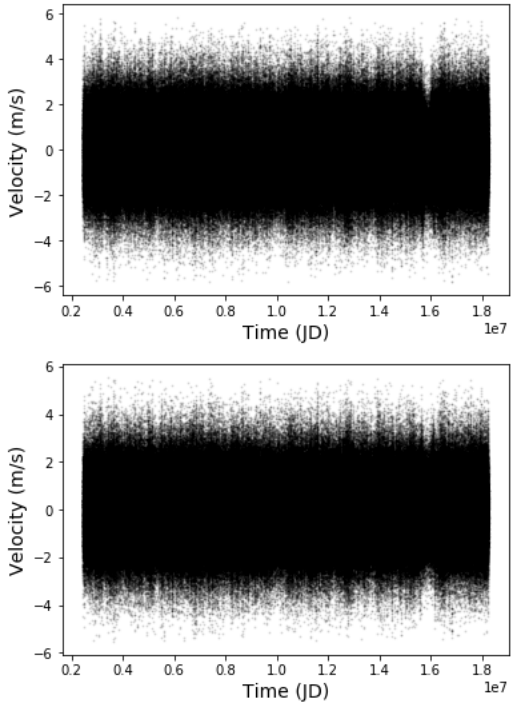

Figure 1: Velocity Dispersion for the first 6 months of GOLF Data (11th April 1996 - October 10th 1996) from Photomultipliers 1 (above) and 2 (below), using calibration method 1.

We note that no large variations of solar activity are salient in the time series. In fact, the data corresponds to a minimum of solar activity and thus forms a coherent observational set. [1]

In figure 2, a 1-hour slice of the time series is shown, where the five-minute oscillations are clearly visible. In a sense, these oscillations first observed in 1962, in the seminal paper [10] are a veritable *birth certificate* [11] of helioseismology.

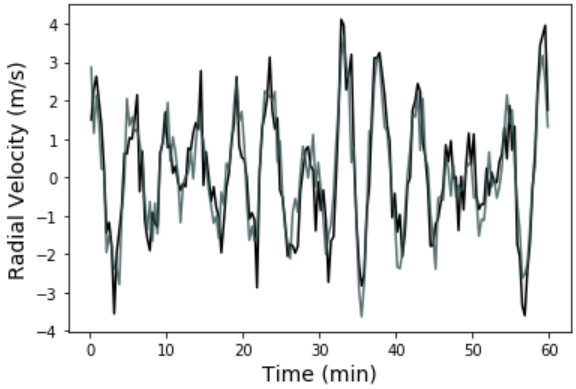

Figure 2: Surface Velocity for the first hour of GOLF Data (11th April 1996 00:00:9.5-01:00:9.5), data from PM1 (black) and PM2 (gray); the 5-minute oscillations are clearly visible.

We analyse the data calibrated using the magnetic modulation of the signal (method 1), rather than the modeling of the photometric response of the detectors (method 2), which extrapolates pre-launch measurements to in-flight conditions.

In figure 3, we plot the surface velocity as measured by one photomultiplier as a function of the measurement of the other, with the maximum correlation shown by a dashed blue line.

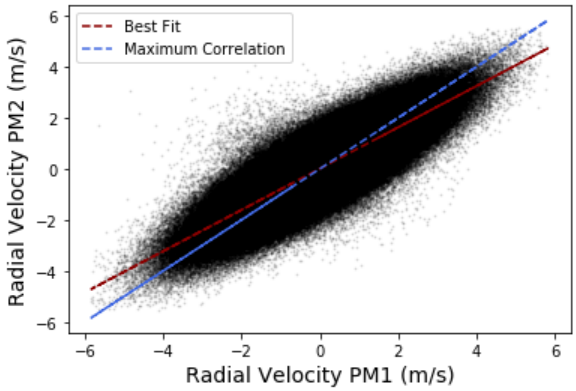

Figure 3: Correlation between the Velocity Dispersions obtained from photomultiplier 1 (PM1) and photomultiplier 2 (PM2), using calibration method 1; the maximum correlation line is shown in blue, and the best linear fit to the data in red.

In the best linear fit to the data (dashed red line), we obtain a slope of (0.8096 ± 0.005) with a reduced chi-square of $\chi^2_\nu = 0.54$, a difference of less than 20% that falls within the error of the calibration method as estimated by [1].

2.2 Solar Oscillation Spectrum

We perform a Fast Fourier Transform of the GOLF surface velocity time series, with a sampling period of 20 seconds. In figure 4, we plot the solar oscillation spectrum thereby obtained for the acoustic modes frequency range (1-5 mHz).

As predicted by the assymptotic results for the frequencies of low-degree acoustic modes, the peaks are regularly spaced. Also, the linewidth of the peaks increases with frequency (and thus with radial order) for data from both photomultipliers.

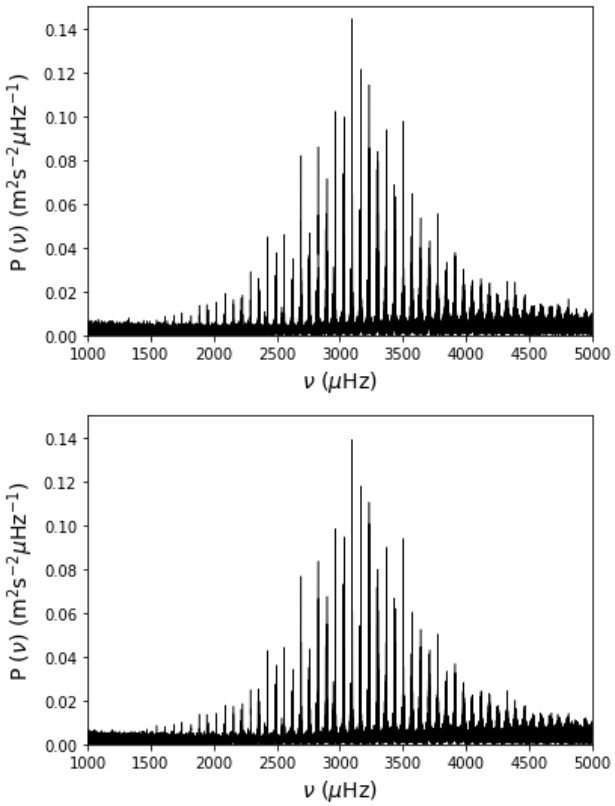

Figure 4: Solar Oscillation Spectrum, from the first six months of GOLF data, in the p-mode range. Power Spectral Density as a function of frequency, for PM1 (above) and PM2 (below).

We note that the spectrum obtained using data from detector PM2 is globally shifted towards lower frequencies compared to PM1; in particular, this is evident for the highest-intensity peak, although the overall shape of the spectra are identical.

Additionally, we observe high-intensity peaks for low frequencies ($f \approx 0$ Hz), plotted in figure 5. Whereas from ground it is very difficult to observe modes with frequencies lower than 2 mHz, which already have lower intrinsic amplitudes, mainly due to *solar noise* from the convection zone [3], in addition to terrestrial noise, from space the threshold for mode identification is shifted to lower frequencies. In figure 4, peaks are distinguishable from noise from $f = 1.5$ mHz.

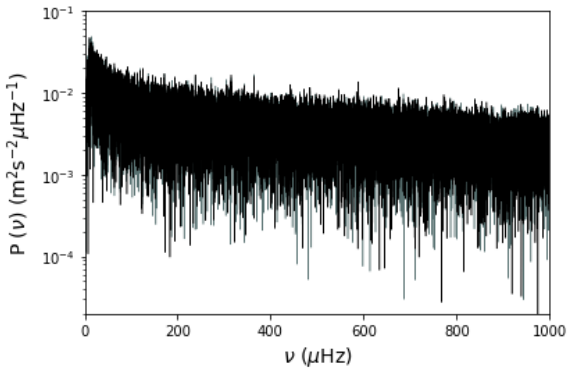

Figure 5: High Intensity Peaks near f $\approx$ 0 Hz in the Solar Oscillation Spectrum for the GOLF data (logarithmic scale), using time series from both PM1 (black) and PM2 (gray).

2.3 Frequency Matching

In figure 6, we compare the theoretical frequencies obtained from modelling of the Sun to those observed in the oscillation spectra using data from both detectors for a slice of the acoustic p-mode range, in the region of highest power density.

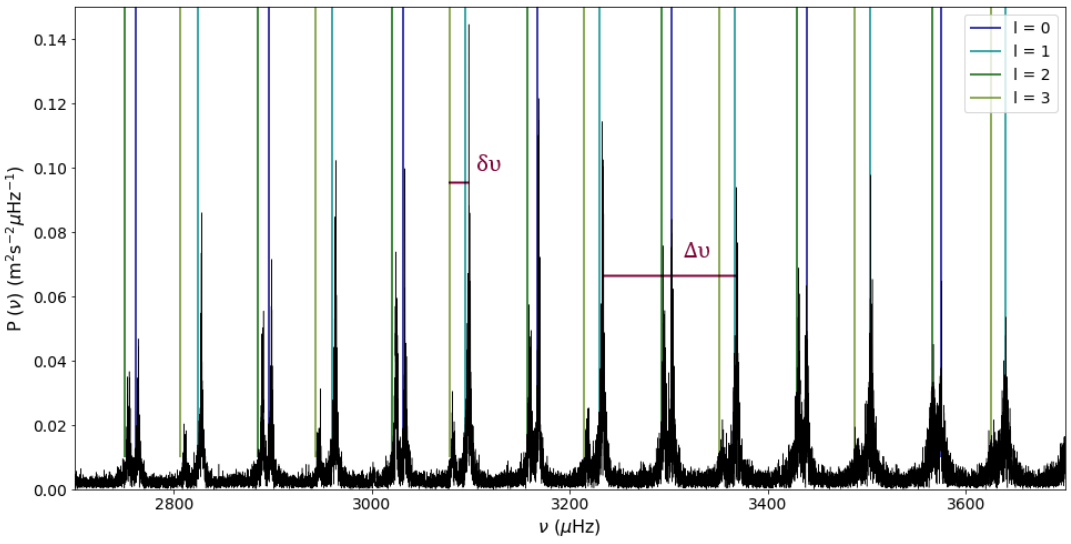

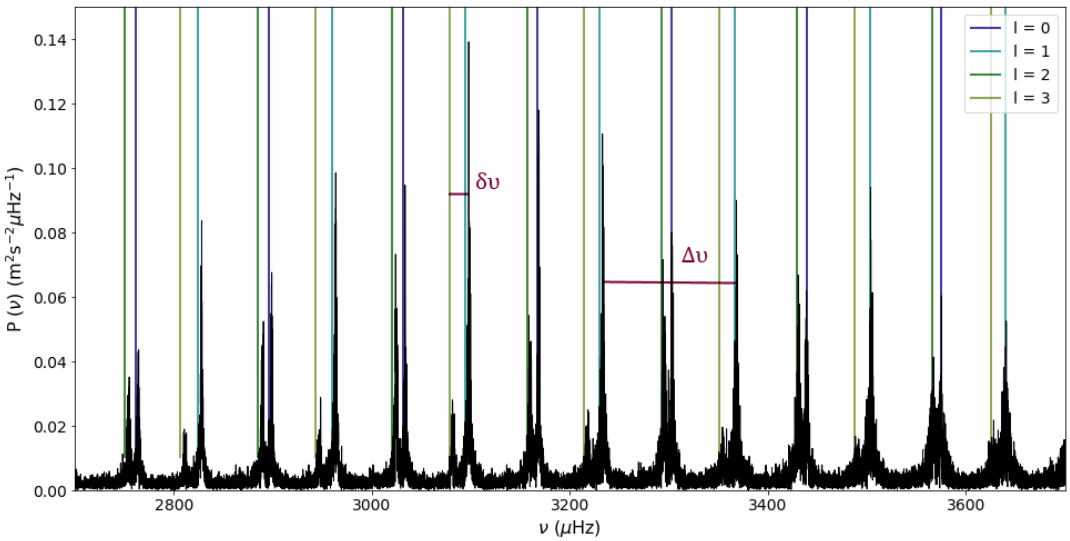

Figure 6: A slice of the solar oscillation spectrum with low-degree theoretical frequencies ($l \leq 3$) with $19 \leq n \leq 24$ superimposed, for PM1 (above) and PM2 (below). In solid red lines, the the small ($\delta\nu$) and large separation ($\Delta\nu$) are shown.

2.4 Large Separation

We compute the large separation predicted from modelling the Sun for $l \leq 3$, in the acoustic p-mode range 1-5 mHz.

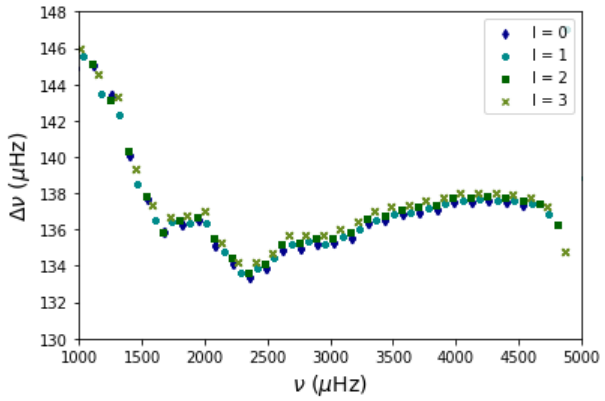

Figure 7: Large Separation as a function of frequency, for $l \leq 3$, using theoretical frequencies from a model of the Sun.

2.5 Small Separation

We also compute the small separation using theoretical frequencies obtained from a solar model, for radial ($l = 0$) and $l = 1$ modes. Clearly, in the range 2-5 mHz, the separation decreases linearly with frequency (and hence with n).

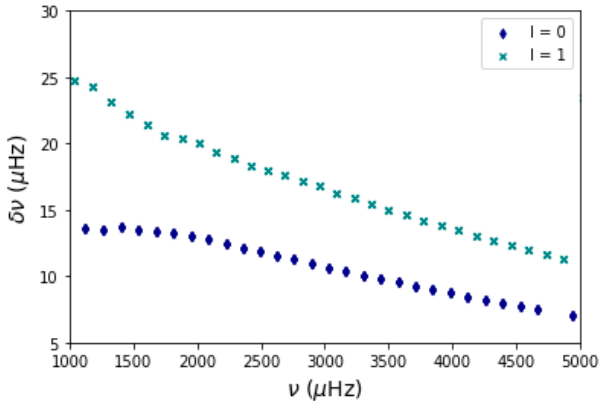

Figure 8: Small Separation as a function of frequency, for $l = 0, 1$, using theoretical frequencies from a solar model.

2.6 Eigenfrequencies of Solar Oscillation

We fit each peak to a Lorentzian function, where the initial guess for ν_0 is the corresponding mode's predicted frequency,

$$L(\nu) = \frac{1}{2\pi} \frac{\Gamma}{(\nu - \nu_0)^2 + (\frac{\Gamma}{2})^2} \tag{7}$$

whose linewidth (full-width at half-maximum) is 4Γ. [12]

We model the background empirically as a quadratic function of frequency ν, so the global fit, shown in red in figure 9 is the sum of the background and each fitted lorentzian peak.

In figure 9, we plot the best least-squares fit to the data for the most penetrating ($19 \leq n \leq 24$) low-degree ($l \leq 3$) modes.

In table 1, we compare the frequencies predicted from modelling the Sun with those obtain by least-square fitting the observed peaks in the Fourier spectrum for these modes.

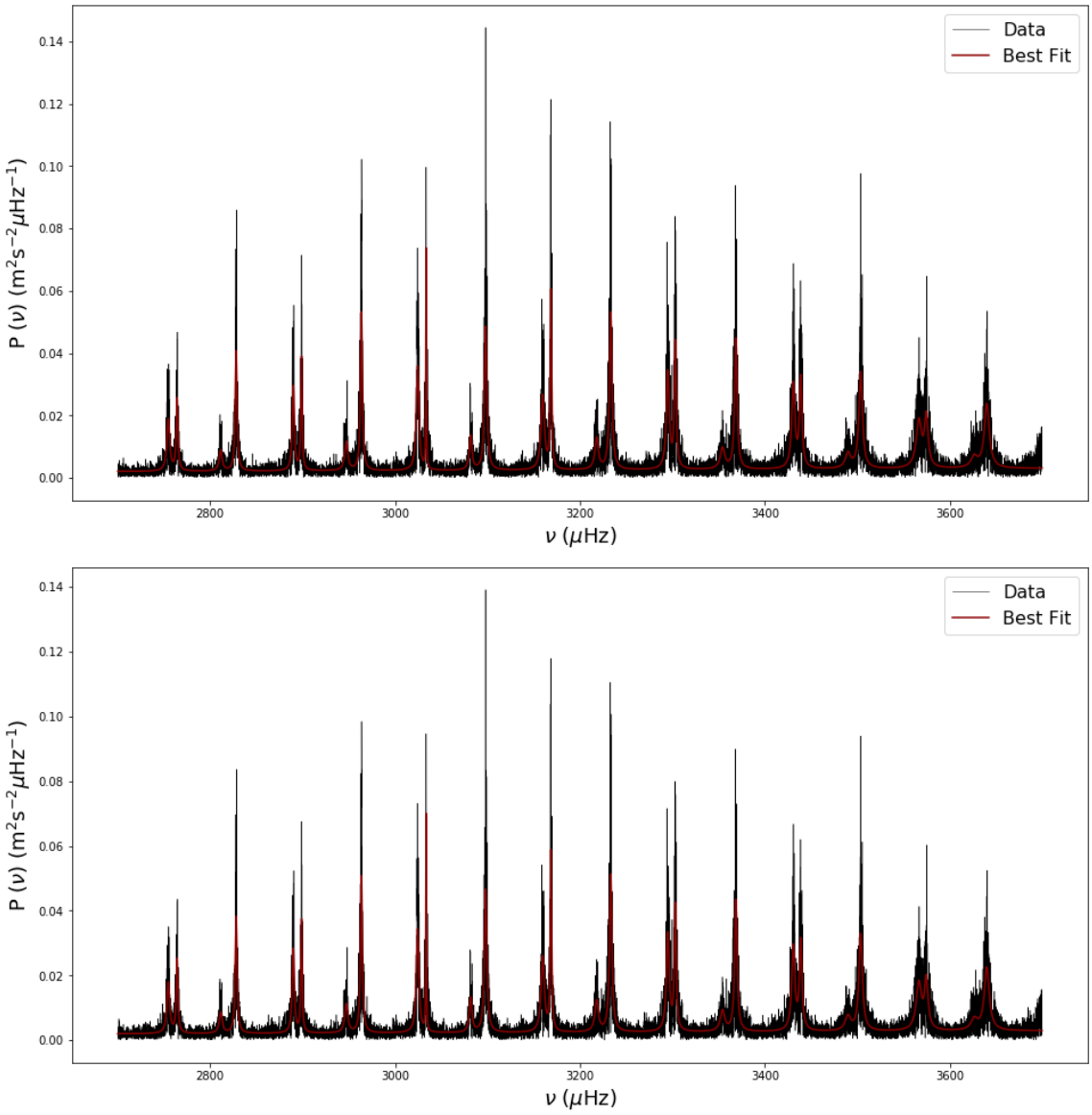

Figure 9: A slice of the global fit to the solar oscillation spectrum for GOLF/SoHO. Data from PM1 (above) and PM2 (below).

We note the high accuracy of the theoretical predictions using MESA/Gyre for the solar oscillation eigenfrequencies, with all errors (in the sense Sun-theory) under $1.5‰$ and within 2σ (expect for the $l = 0,\ n = 21$ mode) of the predicted value.

In figure 10, we plot the relative error $\delta\nu/\nu$ as a function of frequency for the $l \leq 3$ modes in the acoustic frequency range 1.5-4 mHz. We note that the agreement is excellent for the most penetrating modes, and that whereas for low-order modes the predictions are overestimates, the relative error decreases (almost linearly) with frequency so for higher-order modes, they are underestimates of the observed frequencies.

A few outliers are visible in figure 10, whose deviations to the overall error curve may be attributable to acoustic glitches in the sound speed profile, possibly related to the bottom of the convection zone or to He II ionization near the surface [13].

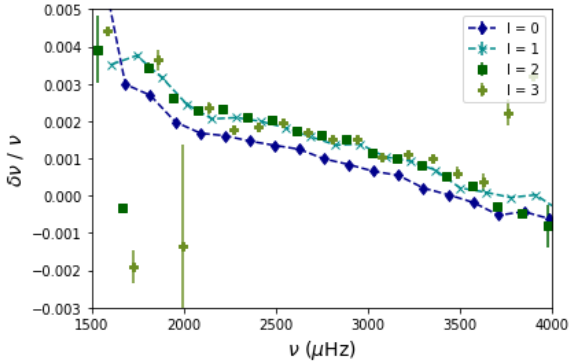

Figure 10: Relative error $\delta\nu/\nu$ (in the sense Sun-theory) as a function of frequency for the observed solar eigenfrequencies.

Degree	Radial Order (n)	Observed (μHz)	Predicted (μHz)	Error (%)	Error (σ)
$l = 0$	19	2764.18(0.07)	2761.45	0.10	1.26
	20	2896.41(0.04)	2898.84	0.08	1.47
	21	3031.63(0.01)	3033.61	0.07	3.15
	22	3166.92(0.02)	3168.65	0.05	1.04
	23	3302.48(0.04)	3303.16	0.02	0.29
	24	3438.83(0.07)	3438.91	0.01	0.03
	25	3575.35(0.15)	3574.70	0.02	-0.14
$l = 1$	19	2828.07(0.04)	2824.23	0.14	1.65
	20	2963.65(0.03)	2959.56	0.14	1.75
	21	3098.02(0.04)	3094.79	0.10	1.07
	22	3233.37(0.04)	3230.37	0.09	0.96
	23	3368.74(0.04)	3366.42	0.07	0.73
	24	3503.70(0.07)	3502.97	0.02	0.16
	25	3640.20(0.13)	3639.85	0.01	0.05
$l = 2$	19	2754.62(0.12)	2750.18	0.15	1.23
	20	2889.84(0.06)	2885.44	0.15	1.64
	21	3024.45(0.06)	3020.98	0.11	1.01
	22	3159.75(0.09)	3156.55	0.10	0.75
	23	3295.12(0.06)	3292.41	0.08	0.73
	24	3430.88(0.08)	3429.03	0.05	0.45
	25	3566.72(0.22)	3565.82	0.03	0.13
$l = 3$	19	2811.33(0.29)	2807.06	0.15	1.14
	20	2947.21(0.22)	2942.79	0.15	1.09
	21	3081.75(0.17)	3078.50	0.11	0.98
	22	3218.11(0.21)	3214.52	0.11	0.81
	23	3354.33(0.37)	3350.93	0.10	0.58
	24	3490.07(0.56)	3487.94	0.06	0.31
	25	3626.54(0.86)	3625.22	0.04	0.16

Table 1: Comparision of the acoustic frequencies for the most penetrating modes observed in the solar oscillation spectrum and predicted using MESA/Gyre; standard errors in the last digits of the fitted frequencies are shown in parentheses.

In figure 11, we plot the observed small separation for the $19 \leq n \leq 25$ modes, and a linear fit to the data, in good agreement for both $l = 0$ ($\chi^2_\nu = 1.20$) and $l = 1$ modes ($\chi^2_\nu = 2.10$); the error bars are magnified 5× for comparision.

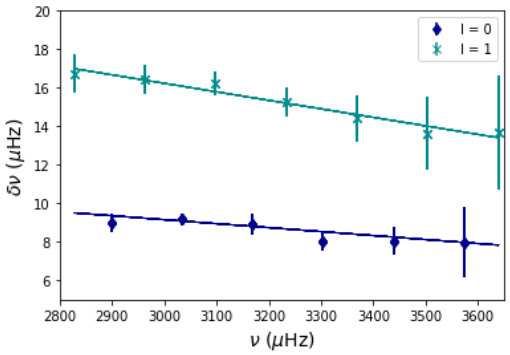

Figure 11: Small Separation $\delta\nu$ as a function of frequency, for the most penetrating modes ($19 \leq n \leq 25$). In solid lines, a linear fit to the data is shown; error bars are magnified 5×

We obtain an average small separation of $\langle\delta\nu\rangle = 8.67 \pm 0.35\,\mu$Hz for the most penetrating radial modes. Using a 120 days time series from VIRGO, with $20 \leq n \leq 22$, [13] obtains an average small separation (weighted by the signal to noise ratio of each peak) of $\langle\delta\nu\rangle_{\text{VIRGO}} = 9.13 \pm 0.05\,\mu$Hz.

Our results are therefore compatible within 1.3σ with [13].

In figure 12, we show the observed large separation for the whole range of low-noise peaks (1.5-4 mHz) and a linear interpolation of the predicted separations in dashed lines.

We obtain an average large separation of $\langle\Delta\nu\rangle = 135.41 \pm 0.66\ \mu$Hz, for the most penetrating $l \leq 3$ modes. Using the aforementioned VIRGO data, and weighting by the signal to noise ratio for $l \leq 2$ modes [13] obtained $\langle\Delta\nu\rangle_{VIRGO} = 135.01 \pm 0.05\ \mu$Hz, a 0.6σ difference from our estimate.

We note the good agreement between theory and predictions, and that the errors are larger for higher frequencies in the $l = 2$ and $l = 3$ modes, likely due to higher uncertainties in fitting the center of the Lorentzians due to a lower signal to noise ratio in the corresponding peaks (see Appendix).

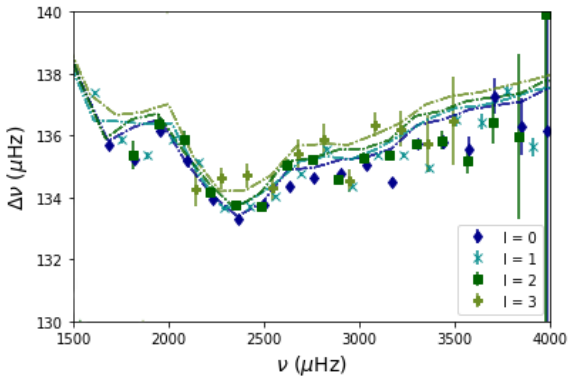

Figure 12: Large Separation as a function of frequency for low-degree p-modes in the range 1.5-4 mHz. In dashed lines, a linear interpolation of the predicted separations is shown.

2.7 Linewidths

In frequency space, each oscillation mode is well-approximated by a Lorentzian curve; the oscillations are damped by surface convection in the Sun, and the width of the curve (parametrized by Γ in equation 7) measures the lifetime of the mode: the faster it decays, the broader the Lorentzian.

We plot the linewidth as a function of frequency in logarithmic scale in figure 13. Clearly, the damping tends to increase with frequency, resulting in broader peaks (and larger linewidhts) at higher frequencies, but the profile is far from monotonous.

A plateau is formed in the range 2500-3000 μHz, with a dip at $\nu \approx 3000\,\mu$Hz (particularly noticeable for $l = 0$), and the linewidths steeply increase at higher frequencies, matching the overall shape of both VIRGO and BiSON data [13].

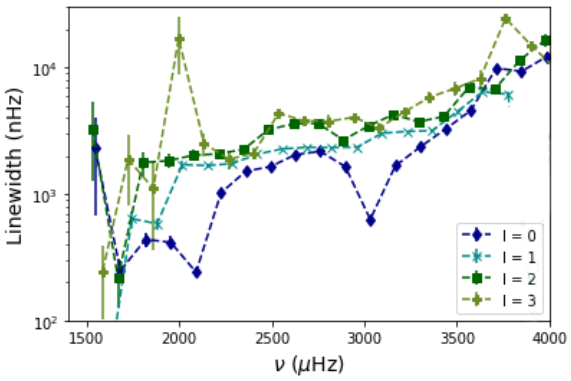

Figure 13: Linewidth as a function of frequency, for the $l \leq 3$ p-modes in the range 1.5-4 mHz (logarithmic scale).

2.8 Echelle Diagram

Since the p-modes of a certain (low) degree l observed in the Sun's oscillation spectrum are expected to be evenly spaced by the large separation $\Delta\nu$, in figure 14, we represent the most penetrating modes modulo the average large separation.

As we expected, the eigenmode frequencies form a roughly vertical ridge in the Echelle diagram for each angular degree.

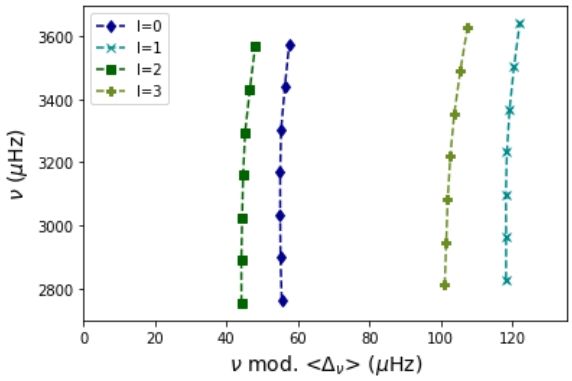

Figure 14: Echelle Diagram for the observed p-mode frequencies, with $l \leq 3$, using the first six months of GOLF data.

3 Conclusions and Future Perspectives

Helioseismology's theory and tools not only lead to an understanding of the structure and dynamics of the Sun through the study of its oscillations, but can be applied to other stars that display stochastic oscillations excited by turbulent convection.

In the determination of stellar parameters, both the large and small separation are useful diagnostics. While the large separation $\Delta\nu$ is sensitive to the density of the star (and hence to its mass and radius), the small separation $\delta\nu$ relates to its age. As the star burns hydrogen and produces helium through nuclear fusion, the mean molecular weight μ increases and, as long as the core temperature remains roughly constant, the sound speed decreases, from equation 6, so does $\delta\nu$. [13]

In the next decades, astroseismological measurements of stars in different evolutionary stages will hopefully enable astrophysicists to better understand their evolution and dynamics.

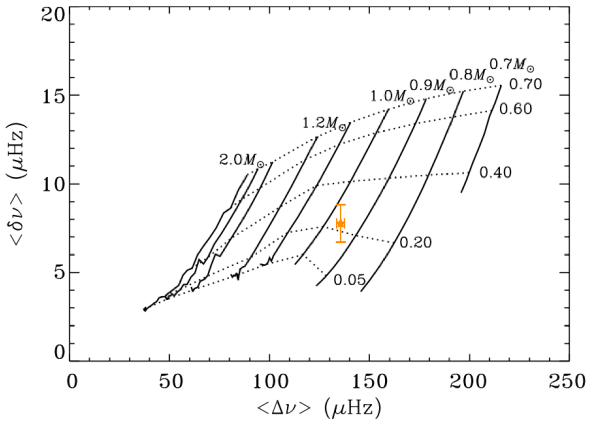

Figure 15: Asteroseismic Hertzsprung-Russell Diagram. Our estimate for the Sun is shown in orange; error bars are 3σ.

References

[1] S. Turck-Chieze et al. “First View of the Solar Core from GOLF Acoustic Modes”. In: Solar Physics 175.2 (1997), pp. 247–265. DOI: 10.1023/a:1004992727541. URL: https://doi.org/10.1023/a:1004992727541.

[2] A. H. Gabriel et al. “Global Oscillations at Low Frequency from the SOHO mission (GOLF)”. In: Solar Physics 162.1-2 (Dec. 1995), pp. 61–99. DOI: 10.1007/bf00733427. URL: https://doi.org/10.1007/bf00733427.

[3] M. Lazrek et al. “First Results on p-modes from GOLF Experiment”. In: Solar Physics 175.2 (1997), pp. 227–246. DOI: 10.1023/a:1004942929956. URL: https://doi.org/10.1023/a:1004942929956.

[4] Rafael A. Garcia et al. “Tracking Solar Gravity Modes: The Dynamics of the Solar Core”. In: Science 316.5831 (June 2007), pp. 1591–1593. DOI: 10.1126/science.1140598. URL: https://doi.org/10.1126/science.1140598.

[5] E. Fossat et al. “Asymptotic ≤i≥g≤ i≥ modes: Evidence for a rapid rotation of the solar core”. In: Astronomy & Astrophysics 604 (Aug. 2017), A40. DOI: 10.1051/0004-6361/201730460. URL: https://doi.org/10.1051/0004-6361/201730460.

[6] Hannah Schunker et al. “Fragile Detection of Solar g-Modes by Fossat et al.” In: Solar Physics 293.6 (June 2018). DOI: 10.1007/s11207-018-1313-6. URL: https://doi.org/10.1007/s11207-018-1313-6.

[7] P. H. Scherrer and D. O. Gough. “A Critical Evaluation of Recent Claims Concerning Solar Rotation”. In: The Astrophysical Journal 877.1 (May 2019), p. 42. DOI: 10.3847/1538-4357/ab13ad. URL: https://doi.org/10.3847/1538-4357/ab13ad.

[8] M. Tassoul. “Asymptotic approximations for stellar nonradial pulsations”. In: The Astrophysical Journal 43 (Aug. 1980), p. 469. DOI: 10.1086/190678. URL: https://doi.org/10.1086/190678.

[9] D. O. Gough. “Asymptotic Sound-Speed Inversions”. In: Seismology of the Sun and the Distant Stars. Springer Netherlands, 1986, pp. 125–140. DOI: 10.1007/978-94-009-4608-8_14. URL: https://doi.org/10.1007/978-94-009-4608-8_14.

[10] Robert B. Leighton, Robert W. Noyes, and George W. Simon. “Velocity Fields in the Solar Atmosphere. I. Preliminary Report.” In: The Astrophysical Journal 135 (Mar. 1962), p. 474. DOI: 10.1086/147285. URL: https://doi.org/10.1086/147285.

[11] J. Bachall. “Ulrich’s Explanation for the Solar Five Minute Oscillations”. In: The Astrophysical Journal 525.C (Nov. 1999), p. 1199. URL: http://www.sns.ias.edu/~jnb/Papers/Popular/Ulrich/paper.pdf.

[12] William Feller. An Introduction to Probability Theory. Second edition. New York: John Wiley & Sons Inc., 1971, pp. xxiv+669.

[13] Thorsten Stahn. “Analysis of time series of solar-like oscillations – Applications to the Sun and HD 52265”. PhD thesis. Mathematisch-Naturwissenschaftlichen Fakultäten der Georg-August-Universität zu Göttingen, 2010.

4 Supplemental Material

We display the best fit to the solar oscillation spectrum for the whole range of frequencies where peaks can be reliably identified in figures 16 and 17. A complete list of the identified frequencies and the code used for the plots is available in this repository.

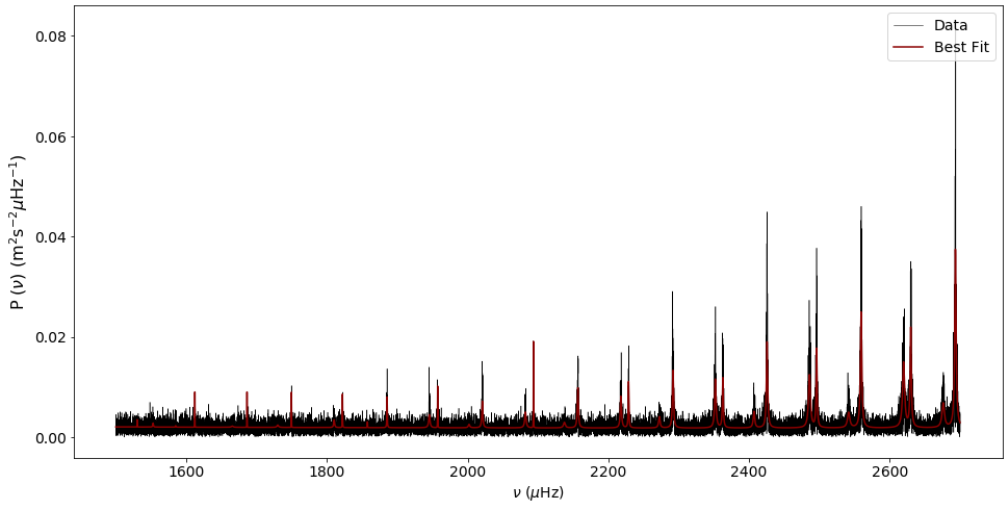

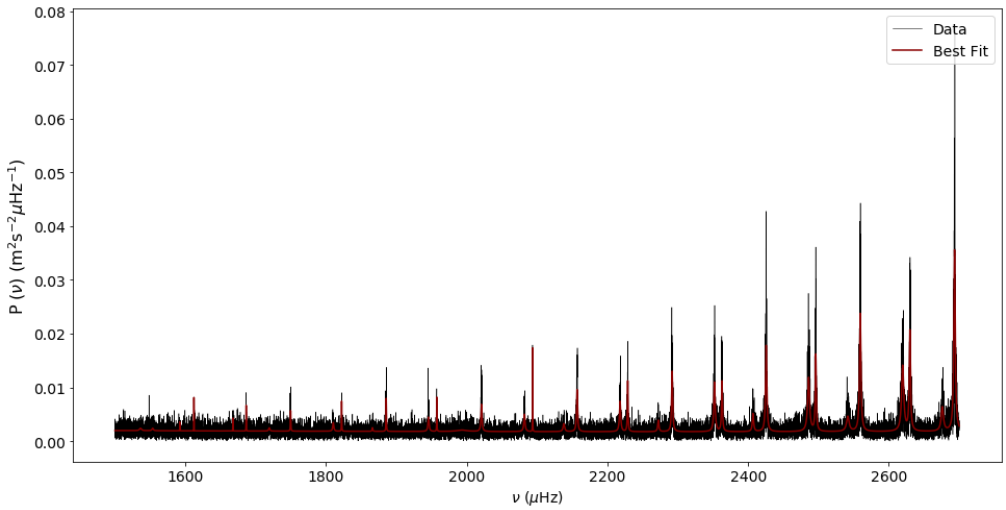

Figure 16: A slice of the global fit to the solar oscillation spectrum, $1500 \leq f \leq 2700$, for PM1 (above) and PM2 (below).

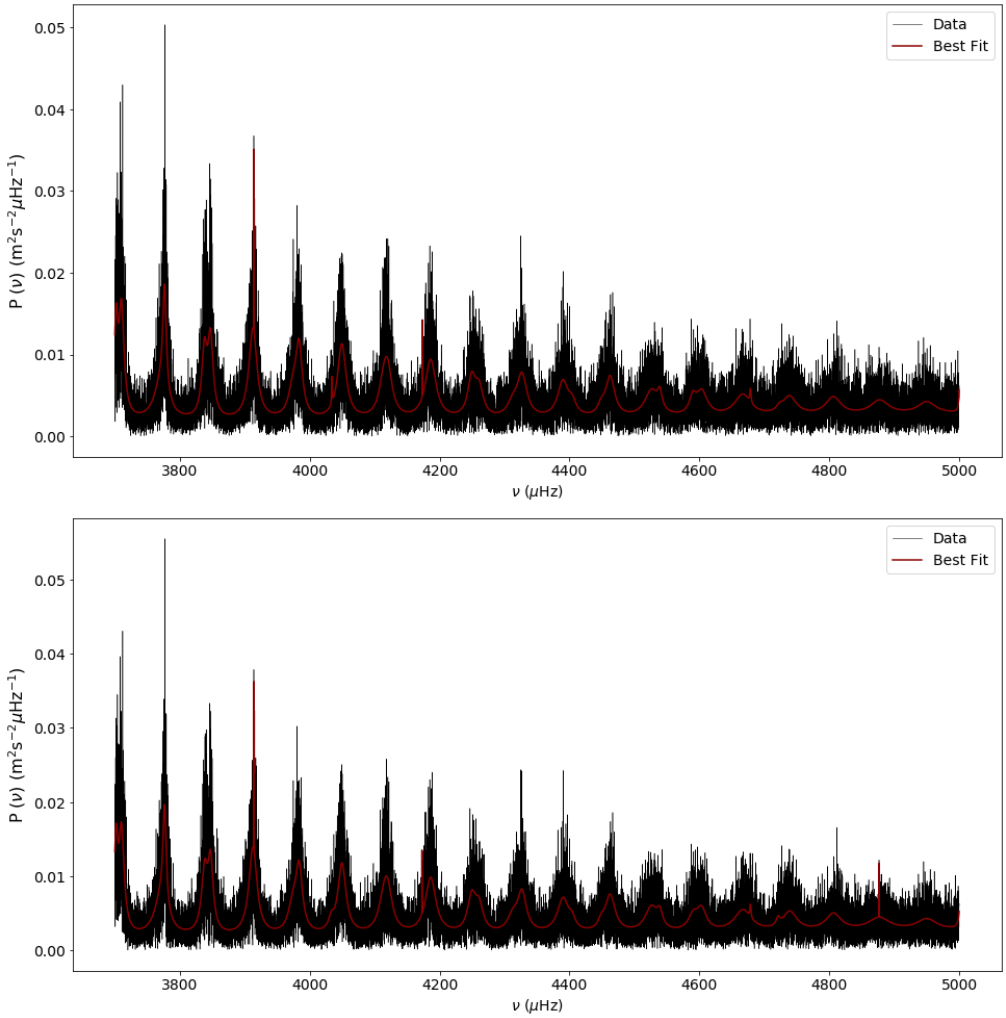

Figure 17: A slice of the global fit to the solar oscillation spectrum, $3700 \leq f \leq 5000$, for PM1 (above) and PM2 (below).